





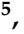




Article

# Parametric Optimization Study of Novel Winglets for Transonic Aircraft Wings

Panneerselvam Padmanathan <sup>1,\*</sup>, Seenu Aswin <sup>1</sup>, Anbalagan Satheesh <sup>1</sup>, Parthasarathy Rajesh Kanna <sup>2</sup>, Kuppusamy Palani <sup>3</sup>, Neelamegam Rajan Devi <sup>4</sup>, Tomasz Sobota <sup>5</sup>, Dawid Taler <sup>5</sup>, Jan Taler <sup>6,\*</sup> and Bohdan Węglowski <sup>6</sup>

- <sup>1</sup> School of Mechanical Engineering, Vellore Institute of Technology, Vellore 632014, Tamil Nadu, India; aswin.ts2018@vitstudent.ac.in (S.A.); satheesh.a@vit.ac.in (A.S.)
- <sup>2</sup> CO<sub>2</sub> Research and Green Technologies Centre, Vellore Institute of Technology, Vellore 632014, Tamil Nadu, India; rajeshkanna.p@vit.ac.in
- <sup>3</sup> Department of Mechanical Engineering, Sri Chandrasekharendra Saraswathi Viswa Mahavidyalaya, Enathur, Kanchipuram 631561, Tamil Nadu, India; palani.k@kanchiuniv.ac.in
- <sup>4</sup> Department of Physics, Auxilium College, Vellore 632006, Tamilnadu, India; devinr@auxiliumcollege.edu.in
- <sup>5</sup> Department of Thermal Processes, Air Protection and Waste Management, Cracow University of Technology, ul. Warszawska 24, 31-155 Cracow, Poland; tomasz.sobota@pk.edu.pl (T.S.); dawid.taler@pk.edu.pl (D.T.)
- <sup>6</sup> Department of Energy, Cracow University of Technology, al. Jana Pawla II 37, 31-864 Cracow, Poland; bohdan.weglowski@pk.edu.pl
- \* Correspondence: padmanathan.p@vit.ac.in (P.P.); jan.taler@pk.edu.pl (J.T.)

**Abstract:** This paper deals with the topic of reducing drag force acting on aircraft wings by incorporating novel winglet designs, such as multi-tip, bird-type, and twisted. The high-speed NASA common research model (CRM) was selected as the baseline model, and winglet designs were retrofitted while keeping the projected wingspan constant. Computational analysis was performed using RANS coupled with the Spalart–Allmaras turbulence model to determine aerodynamic coefficients, such as  $C_L$  and  $C_D$ . It was observed that the multi-tip and bird-type designs performed exceptionally well at a low angle of attack ( $0^\circ$ ). A parametric study was conducted on multi-tip winglets by tweaking the parameters such as sweep angle ( $\Lambda$ ), tip twist ( $\mathcal{C}$ ), taper ratio ( $\lambda$ ), and cant angle ( $\Phi$ ). The best combination of parameters for optimal aerodynamic performance while maintaining the wing root bending moment was determined using both the Taguchi method and Taguchi-based grey relational analysis (T-GRA) coupled with principal component analysis (PCA). Also, the percentage contribution of each parameter was determined by using the analysis of variance (ANOVA) method. At the design point, the optimized winglet design outperformed the baseline design by 18.29% in the Taguchi method and by 20.77% in the T-GRA coupled with the PCA method based on aerodynamic efficiency and wing root bending moment.

**Keywords:** winglets design; transonic flow; optimization; induced drag; Taguchi method



**Citation:** Padmanathan, P.; Aswin, S.; Satheesh, A.; Kanna, P.R.; Palani, K.; Devi, N.R.; Sobota, T.; Taler, D.; Taler, J.; Węglowski, B. Parametric Optimization Study of Novel Winglets for Transonic Aircraft Wings. *Appl. Sci.* **2024**, *14*, 7483. <https://doi.org/10.3390/app14177483>

Academic Editor: Josep Maria Bergada

Received: 4 July 2024

Revised: 16 August 2024

Accepted: 21 August 2024

Published: 23 August 2024



**Copyright:** © 2024 by the authors. Licensee MDPI, Basel, Switzerland. This article is an open access article distributed under the terms and conditions of the Creative Commons Attribution (CC BY) license (<https://creativecommons.org/licenses/by/4.0/>).

## 1. Introduction

Airlines and aircraft manufacturers have been looking for ways to enhance the operational economy of their aircraft since the 1970s, when the price of aviation fuel began to increase dramatically. Engineers started to work on reducing the drag acting on the aircraft, with the notion that this would result in less fuel consumption. Induced drag accounts for 40% and 80% of the overall drag during cruise and take-off conditions, respectively [1]. Winglets have been proven to be the industry's most obvious induced-drag-reducing technology. Winglets are vertical extensions of a plane's wingtips that reduce drag, which increases fuel efficiency, stability, and range and even improves control and handling qualities. Richard Whitcomb initiated research on winglets for commercial aircraft in the mid-1970s. In 1979 and 1980, small, nearly vertical fins were installed on a KC-135A aircraft,

and flight tests were performed [2]. Whitcomb discovered that winglets could improve efficiency by more than 7% in a full-size aircraft [3]. This equates to millions of dollars in fuel expenditures for airlines. This influenced several researchers and engineers to work on novel winglet designs for different aircraft types.

Ali et al. [4] used multi-objective shape optimization to create the best winglet design. The above technique used two objective functions: low drag and structural weight. According to the analysis, fuel weight was lowered by 3.8%, equivalent to 29 million dollars in 15 years for Boeing 747 aircraft. Altab et al. [5] investigated the aerodynamic properties of a wing with winglets at  $0^\circ$  and  $60^\circ$  and no winglets. The  $C_L$  and  $C_D$  were predicted using a fuzzy expert system model, with a relative mean error of 6.52% and 4.74%, respectively.  $C_L$  and  $C_D$  were found to be higher in wings with winglets at a 60-degree angle. Essam et al. [6] analyzed a Cessna wing with a winglet to determine  $C_D$  and  $C_L$  at different cant angles of  $0^\circ$ ,  $30^\circ$ , and  $45^\circ$ . From analyses, wings with winglets increased the lift by 12% and decreased the drag by 4%. Moreover, an 11% improvement in  $C_L/C_D$  was witnessed. Lee et al. [7] studied the winglet dihedral effect on the tip vortex. Winglets with dihedral angles showed reduced vorticity compared to the baseline wing model. Also, the lift-induced drag was reduced after installing a winglet with the dihedral angle to the baseline wing model. Hema et al. [8] modelled the wing of Hydra Technologies' Unmanned Aerial System UAS-S45 Balam and examined its aerodynamics and baseline performance. CFD software was used to calculate the flow field around the Hydra S45 Balam wing. Appending winglets to the wing changed the moment coefficient dramatically.

Many other researchers have also performed comparative studies on different types of winglet shapes. A comparative analysis was performed by Ravikumar et al. [9] between split and blended winglets, using the  $k-\epsilon$  model in Ansys-Fluent. The results showed that blended winglets have better aerodynamic characteristics, high  $C_L/C_D$ , high  $C_L$ , and low  $C_D$  at  $\alpha = 10^\circ$  and  $15^\circ$ . The aerodynamic characteristics of blended and raked winglets were analyzed by Madhanraj et al. [10] at different cant angles and compared with a wing-alone model. A blended winglet at a  $60^\circ$  cant angle was observed to have a high  $C_L/C_D$ . Seshaiyah et al. [11] examined a wing made with the NACA 4412 airfoil, with and without the blended winglet design, using analytical, modelling, and CFD analysis. The results showed that a wing with a winglet can increase the lift-to-drag ( $L/D$ ) ratio by approximately 6% to 15%. A split winglet was modelled by Sohail et al. [12] to improve the aerodynamic characteristics of a wing. It was observed that a split winglet diffused the vortex core more effectively than a simply blended winglet, and aerodynamic performance improved when using a split winglet compared to using a wing without a winglet. Marcel et al. [13] numerically investigated the aerodynamic performance of the wing with single- (blended winglet) and double-winglet (split winglet) designs. The large eddy simulation (LES) method was used for numerical computations since it accurately predicts the transitional flows. The analysis showed that double-winglet configurations performed aerodynamically better than a wing with a single winglet. Andrew et al. [14] created a C-type winglet using numerical optimization methods while considering  $C_L$ ,  $C_M$ ,  $V_{stall}$ , and weight. This wing is useful for tailless aircrafts. Their results showed that the drag was reduced by 15% without considering the structural dynamics. They also analyzed the problems of tip extension with winglets using non-linear optimization.

Several additional researchers investigated various winglet arrangements. Neal et al. [15] performed winglet optimization using numerical methods. Induced drag was obtained using the Trefftz plane method, and a model for profile drag was incorporated with the induced drag optimization method to obtain total drag. Analysis was performed on VSAERO. The geometry was parameterized based on design variables such as root incidence, tip incidence, and the twist of the winglet. João et al. [16] conducted a comparative study between fixed winglets and morphing winglets. In the morphing winglet, camber variation was achieved by changing the angle of the leading and trailing edge. It was found that the camber morphing winglet showed less fuel consumption compared to the fixed winglet. Ishimitsu et al. [17] developed a procedure to design and analyze winglets.

Winglet parameters such as chord-wise location, length, taper ratio, area, sweep, and cant angle were studied on a KC-135 wing. For a winglet with a length of 0.135 times the wing's semi-span, a cant angle of  $20^\circ$  reduced the induced drag by 17%, increasing WRBM by 6%. Winglets reduced the overall drag of the KC-135 wing by 6.2%. Panagiotou et al. [18] conducted computational analysis on a medium-altitude long-endurance (MALE) unmanned aerial vehicle (UAV) with winglets. The study was performed using the Spalart–Allmaras turbulence model. The flow around the wing–winglet was analyzed at first, followed by an investigation of the entire aircraft. Based on different aerodynamic parameters and root bending moments, the winglet design was optimized for height, sweep angle, cant angle, toe angle, etc. Better aerodynamic performance was found after optimizing the initial winglet design, which increased the total flight time by approximately 10%. A blended winglet was designed with design variables such as cant, sweep angle, and height by Haddad et al. [19]. After thorough analysis, a winglet with a cant angle of  $45^\circ$  and a height of 15% of the wing's semi-span was considered the best design. At its design condition, a net drag reduction of 4.8% was observed at Mach 0.7 and 2.5% at Mach 0.8. Catalano et al. [20] examined multi-tip winglets with three tip-tail winglets without a sweep angle. Analysis was performed at different cant angles and angles of attack combinations. The result showed that those winglets at cant angle  $+45^\circ$ ,  $+15^\circ$ , and  $-15^\circ$  showed better aerodynamic performances than other configurations. Smith et al. [21] conducted an experimental study on multi-winglets. Due to the nature of the up-flow at the wingtip, it was determined that a negative geometric twist with negative root incidence must be used in addition to dihedral to ensure that the winglet is working at optimal conditions. The leading winglet provides lift by having a moderate positive angle of attack with respect to the effective flow velocity at the wingtip. Andrew et al. [22] investigated the effects of adding numerous active winglets to an existing UAV to improve cruising and maneuvering performance. When comparing a wing with multiple winglets to a baseline wing with the same aspect ratio, it was proven that a wing with multiple winglets can boost range and endurance by up to 40%. Keizo et al. [23] describe a multidisciplinary design exploration technique for a commercial jet aircraft winglet design that included high-fidelity analysis. From the Pareto front generated in this analysis, the winglet's large cant angle was favourable for both block fuel and maximum take-off weight. Liang et al. [24] developed a winglet design for a solar aircraft using a multi-constrained optimization method. Moreover, the effect of winglets was compared for wings with different aspect ratios. It was concluded that winglets incorporated into wings with an aspect ratio of 29 have detrimental effects on wings. It was also observed that wings with an aspect ratio greater than 15 require winglets with small cant angles and larger cant angles for an aspect ratio less than 10 for optimal performance.

Most of the above-cited works showed comparative studies carried out on winglets such as blended, elliptical, raked, and split [5,6,8–10,13,19] types, which are generally used in the aviation industry. Some worked on unconventional winglet designs, such as multi-tip, morphing winglet, and C-wing [12,14,16,20–22], and they claim that their performance is superior to existing winglet designs. However, there is not enough comparison between these unconventional designs. Moreover, the influence of design parameters on aerodynamic efficiency has also not been much discussed. Although there is much research work on winglet designs, comparing the studies with each other has not been possible due to the use of different wing baseline wing models with different dimensions and configurations like tapered wings, rectangular wings, etc. [5,6,10,13]. Furthermore, many authors [3,5–7,10,12,20] analyzed their designs in the subsonic regime; however, commercial aviation requires design analysis in the transonic regime. Many researchers purely focused on the aerodynamics of the winglet design [6,7,9,10,12,13,16]. However, they did not consider offsetting factors such as wing root bending moment and net weight increment of the model. This study's objective is to tackle the induced drag issue on commercial aviation aircraft. A transport transonic wing model, NASA's common research model, was selected as the baseline wing model, which cruises at 0.85 M [25,26] and a

Re of 40 million. In the first stage of this work, unconventional winglet designs such as twisted, bird-type, and multi-tip winglets were designed and analyzed on ANSYS Fluent V2020. The optimal one was determined by comparing their aerodynamic coefficients such as  $C_L$  and  $C_D$  for varying angles of attacks. In the second stage, the influence of design parameters such as cant, sweep, tip twist angle, and taper ratio on multi-tip winglets was also determined to understand the relative importance of each parameter. The best combination of parameters for optimal performance was determined using the Taguchi method. Moreover, the significance of each parameter was determined by the analysis of variance (ANOVA) method [27].

## 2. Wing and Winglet Models

### 2.1. Baseline Wing Model

A transonic supercritical wing was developed as a common research model (CRM) for CFD validation studies by NASA and Boeing, as shown in Figure 1. The geometry and properties of the model are well established for a nominal 1-G wing at cruise. It is a low-wing configuration that cruises at 0.85 M and  $C_L = 0.5$  ( $Re = 4 \times 10^7$ ,  $C_{ref} = 7$  m and  $S_{ref} = 383.69$  m<sup>2</sup>) [28].

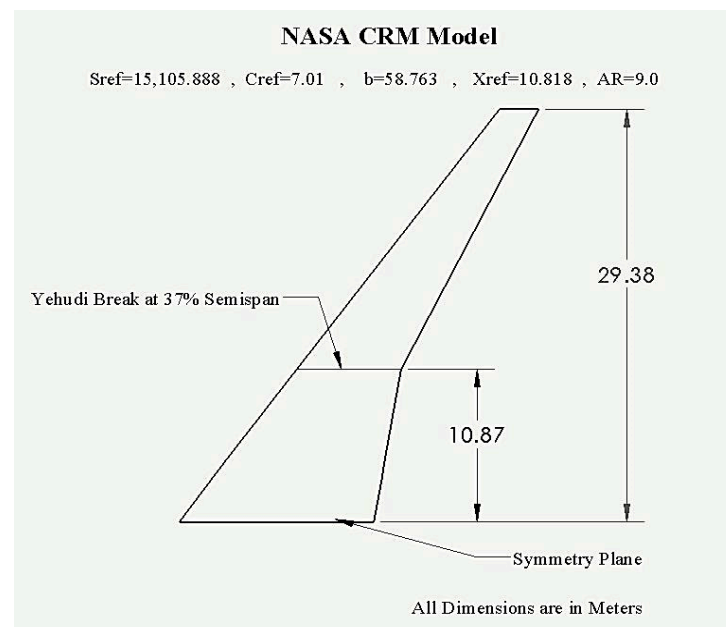


**Figure 1.** NASA CRM wing model.

### 2.2. Conventional and Proposed Winglets

All winglets were designed based on the constraint that the projected wingspan be constant. Conventional winglets such as raked, blended, and wingtip fence winglets were modeled by referring to multiple research papers [6,8–10,13,19,29,30]. The designs from the mentioned literatures were used for comparison with this study's novel winglet designs. The dimensions of the conventional designs are shown in Figure 2. The proposed and novel winglet designs such as twisted, multi-tip, and bird-type were modelled by representing the nature of a bird's feather, as shown in Figure 3. The finger-like wingtips of birds help reduce induced drag by creating small vortices on each tip than forming a big vortex at the wingtips, which generally occurs in aircraft.

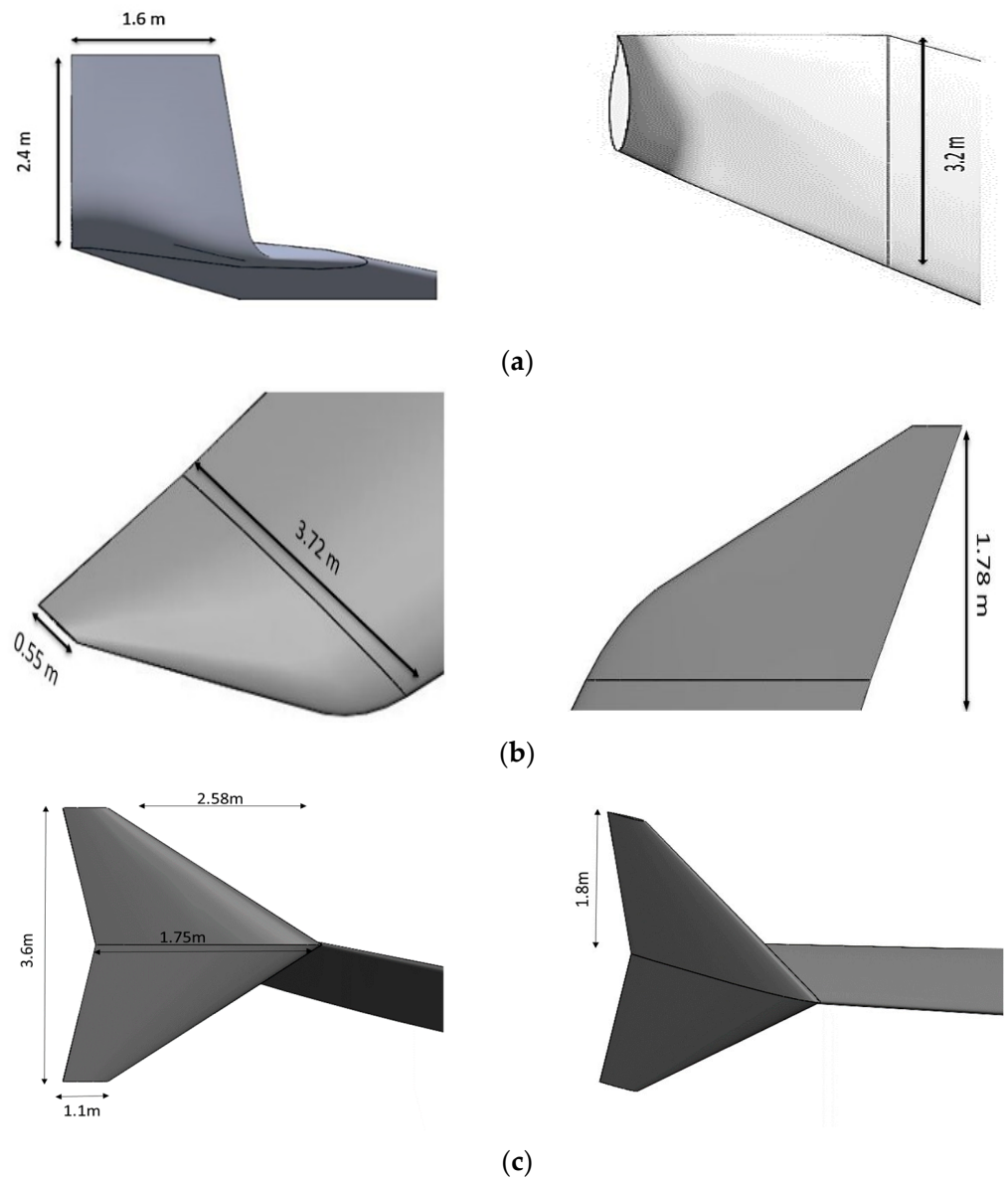


**Figure 2.** A Schematic of (a) blended, (b) raked, and (c) fence winglets.

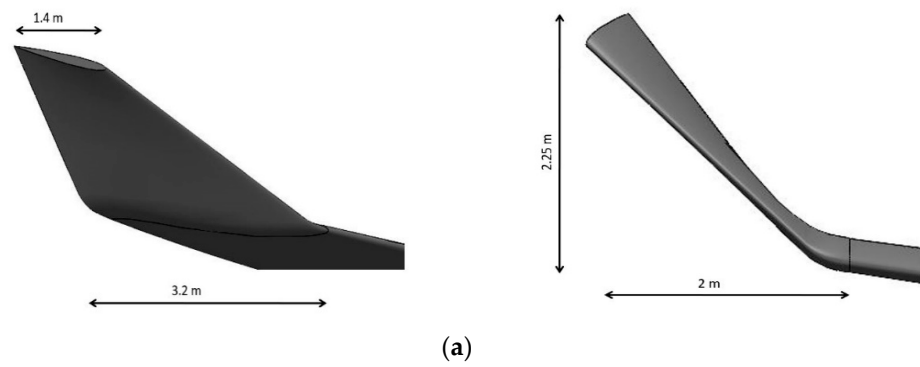


**Figure 3.** Cont.

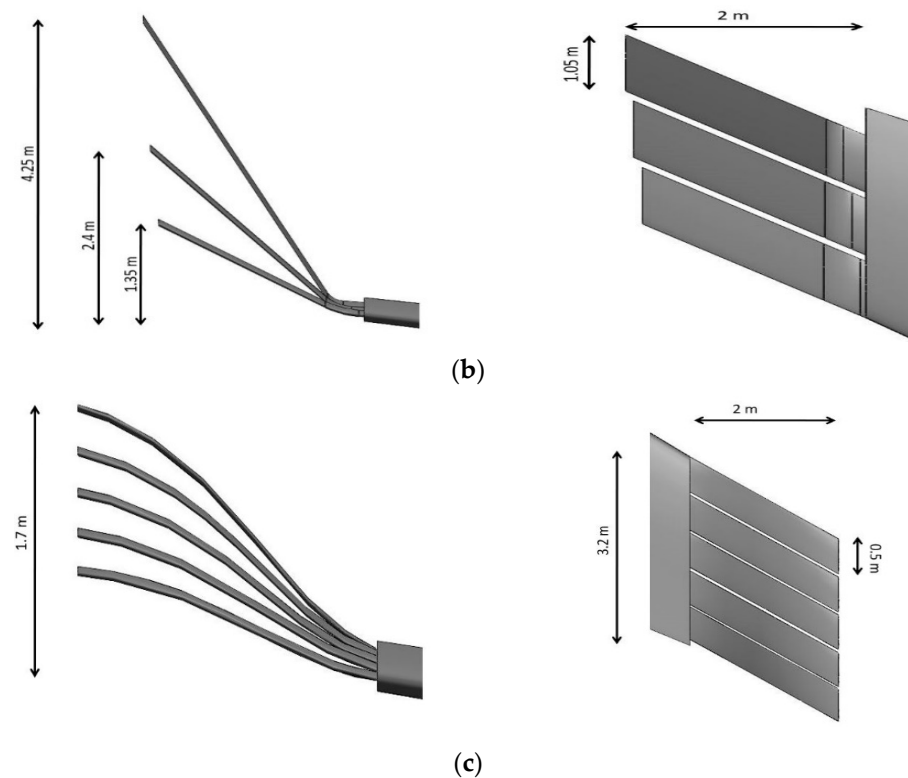


**Figure 3.** A Schematic of (a) twisted, (b) canted multi-tip, (c) and bird-type swept-back winglets.

It has been witnessed that twisted, multi-tip, and bird-type winglets have great potential in reducing drag; thus, these designs were considered for this work. Multi-cant angles give a better aerodynamic performance at a different angle of attack, and thus, multi-tip and bird-type winglets enhance drag reduction. Twisted winglets help in reduction in the wing root bending moment and also tip by being at a negative angle of attack, which stall late compared to the root of the wing.

### 3. Methodology

Airflow is represented as an unsteady, three-dimensional, compressible flow. The governing equations are continuity, x, y, and z-directional Navier–Stokes equations and energy equations. As it would be difficult to solve Navier–Stokes equations due to fluctuating components in the flow field throughout time, a decision was made to use the RANS equation. To solve the closure problem in the RANS equation, the Spalart–Allmaras model is used, as it was created expressly for aerospace applications [31], and it has been proven to perform well for boundary layers subjected to pressure gradients. It simply requires the solution of one transport equation, kinematic turbulent viscosity, which reduces computational complexity. Moreover, the Spalart–Allmaras model [32] has been thoroughly verified for exterior flows and shows good agreement with experimental data in aerospace applications. This study’s computational domain and mesh generation are shown in Figures 4 and 5.

Different computation domain sizes, number of elements, number of inflation layers, and their thickness are tested to obtain accurate results at a fair computational time. The domain size of  $150\text{ m} \times 60\text{ m} \times 60\text{ m}$  with tetrahedron elements is finalized for further computation. Near the winglet, 20 numbers of inflation layers with a first-layer element thickness of 0.1 mm and a growth rate of 1.2 are considered to accurately capture the flow characteristics within the boundary layer. A convergence criterion of  $10^{-6}$  is adopted for obtaining accurate results.

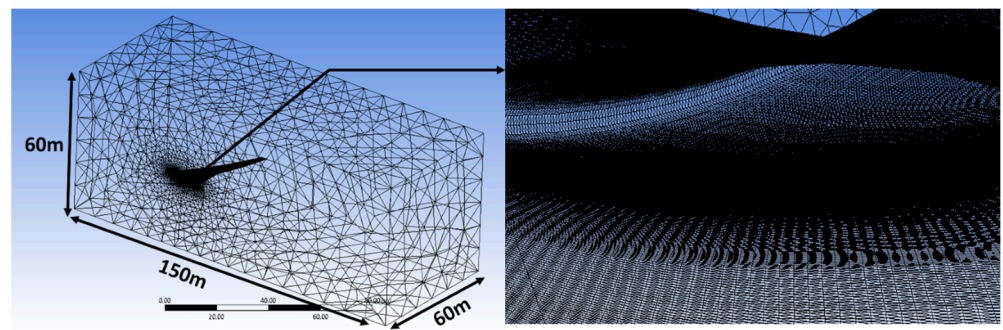


Figure 4. A schematic of NASA CRM mesh.

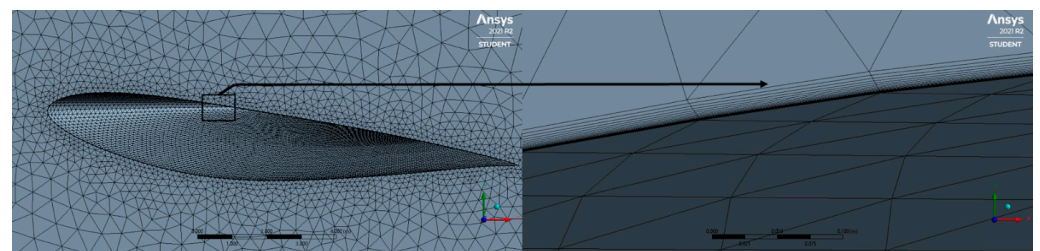


Figure 5. Meshing of inflation layer for this present numerical study.

### 3.1. Validation

The test case of transonic flow over the ONERA M-6 wing [33] is predominantly used for validation purposes by numerous researchers. Therefore, the present computational method is compared with existing research on the ONERA M-6 wing. Analyses are performed for the flow conditions mentioned in Table 1. The  $C_L$  and  $C_D$  of this study are compared with Crovato et al. [34], Durrani et al. [35], Moigne et al. [36], Neilsen et al. [37], and Rho et al. [38], Radespiel [39], Hyoungjin and Oh-Hyun [40] the maximum deviations for both the cases are in the acceptable range of around 6.98% and 7.13% respectively. Furthermore, the computational results are compared with experimental results [34] conducted by the AGARD (Advisory Group for Aerospace Research and Development). The  $C_p$  vs.  $X/C$  graph is plotted at a semi-span of 44% from the root chord, as shown in Figure 6, and the results are in good agreement.

Table 1. Validation of this study with the reported literature.

Flow Condition: $M = 0.8395$ , $Re = 11.72 \times 10^6$ , $\alpha = 3.06^\circ$				
References	$C_L$	$C_D$	$C_L$ Error (%)	$C_D$ Error (%)
This present study	0.2543	0.0181	-	-
Crovato [34]	0.2720	0.0181	6.98	0
Durrani [35]	0.2540	0.0191	0.10	5.58
Moigne [36]	0.2697	0.0174	6.08	4.04
Neilsen [37]	0.253	0.0168	0.49	7.13
Rho [38]	0.2622	0.0175	3.13	3.21
Flow Condition: $M = 0.84$ , $Re = 11 \times 10^6$ , $\alpha = 3.06^\circ$				
References	$C_L$	$C_D$	$C_L$ Error (%)	$C_D$ Error (%)
This present study	0.2527	0.0175	-	-
Radespiel [39]	0.2677	0.0178	5.93	1.77
Hyoungjin and Oh-Hyun [40]	0.2550	0.0161	5.6	1.72

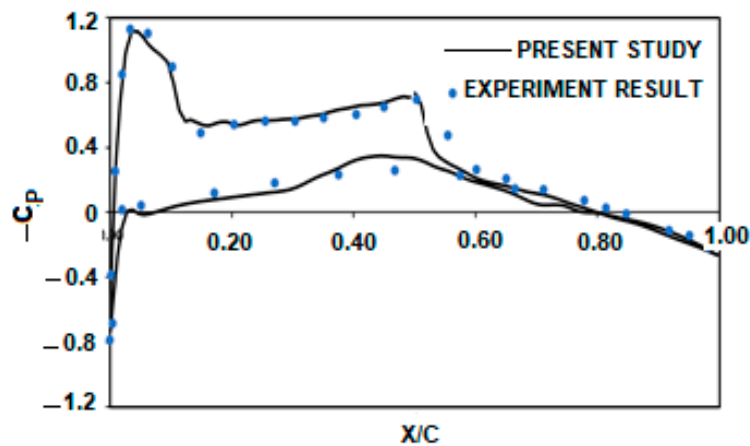


**Figure 6.** Validation of this present study with the AGARD's experimental results [33].

### 3.2. Grid Independent Test

A grid independent test is performed by determining  $C_L$  and  $C_D$  for the NASA CRM wing, baseline wing model. The number of elements varied from 0.5 million to 4 million with an increment of 0.5 million. The graphs are plotted between aerodynamic coefficients, and the number of elements as shown in Figure 7. The deviation of  $C_L$  and  $C_D$  between 2 million and 2.5 million elements are 0.74% and 0.55%, respectively. Therefore, the 2 million elements are used for the rest of the computational analyses.

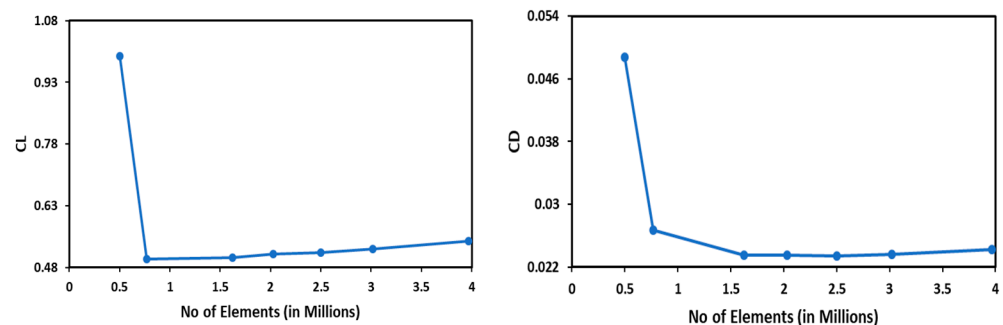


**Figure 7.** Results of grid independent test.

## 4. Results and Discussion

### Aerodynamic Analyses of Winglet Designs

Winglet designs are analyzed at 0.85 M and a Re of  $40 \times 10^6$  ( $C_{ref} = 7$  m and  $S_{ref} = 191.845$  m<sup>2</sup>) for angles of attack at  $0^\circ$ ,  $5^\circ$ , and  $10^\circ$ . Aerodynamic coefficients such as  $C_L$  and  $C_D$  are noted and compared with the baseline model, as shown in Table 2. It can be observed from Table 2 that the twisted, multi-tip, and bird-type winglets outperform other types of winglets with improved  $C_L/C_D$  for all three attack angles. From the results shown in Figure 8, it is evident that a multi-tip winglet at a zero-degree angle of attack outperforms other winglet designs, and its aerodynamic efficiency is 23.47% better than the baseline model, followed by the bird-type winglet with an improvement of 22.83%. At a  $5^\circ$  angle of attack, bird-type, twisted, and multi-tip winglets show improvement in  $C_L/C_D$  by 4.53%, 3.05%, and 1.89%, respectively. At a higher-degree angle of attack,  $\alpha = 10^\circ$ , the bird-type winglet performs better than the baseline model by 0.67%. The aerodynamic efficiency decreases as  $\alpha$  increases due to increased drag [39]. In particular, the multi-tip and bird-type winglets have positive twist angles, thus leading them to stall at higher  $\alpha$ . An appropriate twist angle at the wingtips could resolve this issue. It is concluded from the first-stage analyses that multi-tip and bird-type winglets perform better than the other designs. Although the bird-type winglet performs marginally better than the multi-tip winglet, the parametric study is conducted on the multi-tip winglet, as it is relatively easier



to parameterize the design [40]. The flow over each design is investigated using streamline, pressure contour, and vortex core, as shown in Figure 9. The presence of shockwave is observed along the mid-span of the wing. It is also observed that there is no sudden drop in velocity and rise in pressure over the multi-tip winglet, thus resulting in less wave drag compared to other winglet designs.

**Table 2.** Comparison of NASA CRM with different winglets.

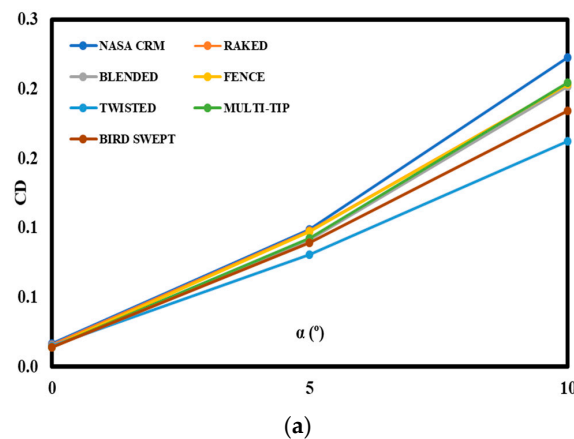
Type	$\alpha = 0^\circ$				
	$C_L$	$C_D$	$C_L/C_D$	Improvement (%) $C_D$	Improvement (%) $C_L/C_D$
NASA CRM	0.3612	0.0169	21.3630	NA	NA
Raked	0.3702	0.0158	23.4304	−6.51	9.68
Blended	0.3412	0.0143	20.1656	−15.39	11.69
Fence	0.3471	0.0146	23.7090	−13.61	10.98
Twisted	0.2754	0.0149	18.4433	−11.83	−13.67
Multi-tip	0.3640	0.0138	26.3768	−18.34	23.47
Bird-type	0.3674	0.0140	26.2393	−17.16	22.83

Type	$\alpha = 5^\circ$				
	$C_L$	$C_D$	$C_L/C_D$	Improvement (%) $C_D$	Improvement (%) $C_L/C_D$
NASA CRM	0.9564	0.0990	9.6630	NA	NA
Raked	0.9540	0.0980	9.7347	−1.01	0.74
Blended	0.8924	0.0913	9.774	−6.76	1.15
Fence	0.8770	0.0974	9.004	−1.6	−0.07
Twisted	0.8054	0.0809	9.9580	−18.28	3.05
Multi-tip	0.9111	0.0925	9.8455	−6.57	1.89
Bird-type	0.899	0.089	10.1011	−10.10	4.53

Type	$\alpha = 10^\circ$				
	$C_L$	$C_D$	$C_L/C_D$	Improvement (%) $C_D$	Improvement (%) $C_L/C_D$
NASA CRM	1.1854	0.2226	5.3252	NA	NA
Raked	1.0760	0.2036	5.2849	−8.54	−0.75
Blended	1.078	0.202	5.3366	−9.25	0.21
Fence	1.0783	0.2031	5.3092	−8.76	−0.30
Twisted	0.6732	0.1624	4.1451	−27.04	−22.16
Multi-tip	1.0737	0.2042	5.2585	−8.27	−1.25
Bird-type	0.9885	0.1844	5.3606	−17.16	0.67



**Figure 8.** Cont.

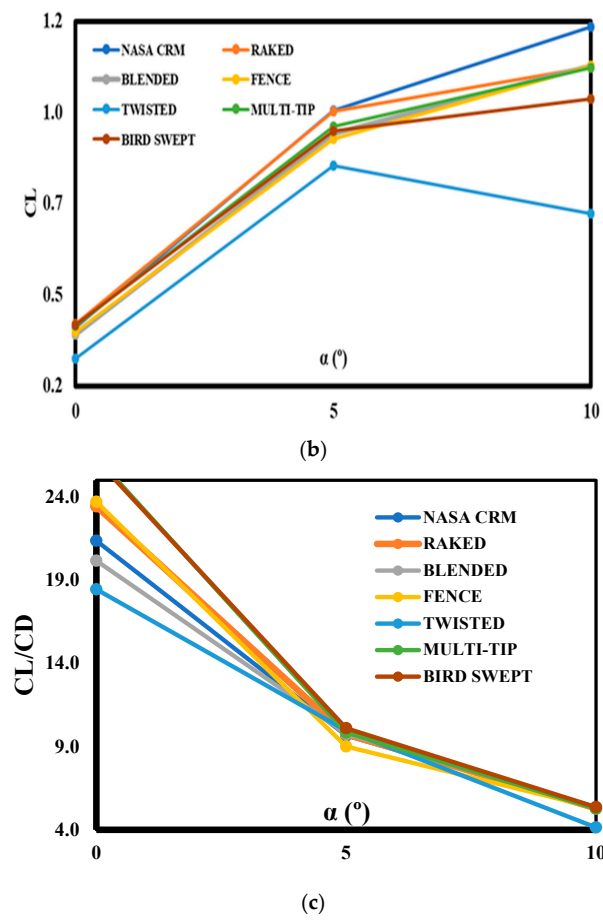


Figure 8. The effect of attack angles on (a) drag coefficient, (b) lift coefficient, and (c)  $C_L/C_D$  for different winglet designs.

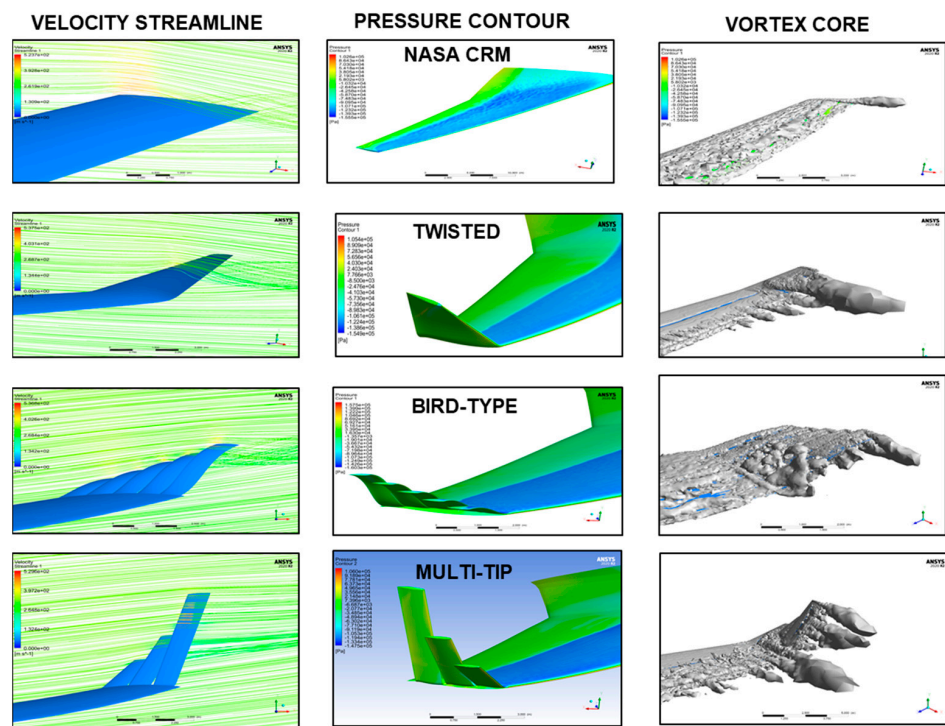


Figure 9. Contours of streamline, pressure, and vortex core for different winglets.

## 5. Optimization Studies

Winglet design predominantly depends on parameters such as cant angle, twist angle, sweep angle, and taper ratio. These parameters influence the  $C_L$ ,  $C_D$ , and  $C_M$  significantly. However, there is insufficient evidence on how much each parameter influences them. Therefore, a parametric study is conducted using the Taguchi technique to understand the relative performance of each parameter and to determine the combination of parameters for an optimal design. Moreover, ANOVA is used to determine the percentage contribution of each parameter.

### 5.1. Parameter Selection

Through a thorough literature review, the top four important parameters are identified and mentioned in Table 3. Although the number of tips is an important parameter, a decision was made to not include it in the parametric study due to dependency on the cant angle. Therefore, the number of tips is kept constant beforehand. It is observed that a three-tip design performs better than others (two- and four-tip), as it is able to reduce induced drag while not increasing the wetted area much, i.e., parasite drag [39].

**Table 3.** Selected design parameters and their levels.

Design Parameters	Symbol	1st Level	2nd Level	3rd Level	4th Level
Cant angle of the first tip	$\Phi$	0°	25°	50°	75°
Taper ratio	$\lambda$	0.2	0.4	0.6	0.8
Sweep angle	$\Lambda$	10°	25°	45°	60°
Tip Twist	$\epsilon$	−8°	−6°	−4°	−2°

The chosen winglet has a three-tip configuration. Hence, three cant angles are required to define the design. However, it increases the number of parameters, which further complicates the analysis. Hence, an equation is developed to ensure all tip cant angles are dependent on the first tip's cant angle. It has been noted that the tips are aligned with the same increment in cant angle with each other. Moreover, the optimal increment angle is found to be 10 degrees [21,22]. Thus, equations are developed as shown below.

If  $x$  is the  $\Phi_{First\ tip}$

$$\Phi_{Second\ tip} = (x - 10) \quad (1)$$

$$\Phi_{Third\ tip} = (x - 20) \quad (2)$$

### 5.2. Taguchi Method

The achieved signal-to-noise (S/N) ratio, which employs Taguchi analysis to detect the loss in quality of the variables in diverse issues, indicates the relative significance of the parameters and their ideal combination. The nature of variability and the mean of the quality characteristics are considered simultaneously by both quality loss and variables of the S/N ratio [41]. Moreover, this approach helps researchers focus their attention on quality losses or the SN ratio when solving multi-objective optimisation problems, which has led to an increase in the interest in reducing complexity.

In this study, four winglet design parameters of a transonic wing, namely, cant angle of the first tip, taper ratio, sweep angle, and tip twist, are selected with four levels. The range of the selected design parameters is decided by taking reference from the research paper [24] and is listed in Table 3. CFD analysis is performed, employing the Taguchi L16 orthogonal array for the 16 conditions listed in Table 4 to determine  $C_L$ ,  $C_D$ , and  $C_M$  (bending moment of wing root chord at quarter chord location).

**Table 4.** Taguchi L16 orthogonal array.

Trial No.	Factors			
	$\Phi$ (°)	$\lambda$	$\Lambda$ (°)	$\epsilon$ (°)
1	0	0.2	10	−8
2	0	0.4	25	−6
3	0	0.6	45	−4
4	0	0.8	60	−2
5	25	0.2	25	−4
6	25	0.4	10	−2
7	25	0.6	60	−8
8	25	0.8	45	−6
9	50	0.2	45	−2
10	50	0.4	60	−4
11	50	0.6	10	−6
12	50	0.8	25	−8
13	75	0.2	60	−6
14	75	0.4	45	−8
15	75	0.6	25	−2
16	75	0.8	10	−4

Analyses for the 16 models are performed at the design point,  $C_L = 1$  ( $S_{ref} = 191.845 \text{ m}^2$ ) at  $\alpha = 5.53^\circ$ , of the NASA CRM, and they are tabulated as shown in Table 5. The design point's angle of attack, which is  $5.53^\circ$ , was determined through interpolation, as shown in Figure 10. For design optimization, the larger-the-better criterion is selected for  $C_L/C_D$ , and the smaller-the-better criterion is selected for the absolute  $C_M$ . S/N ratios and the significance of each parameter in each case have been tabulated as shown in Tables 6–8. Figures 11–13 graphically represents the effect of individual design parameter on the S/N ratio for  $C_L/C_D$ ,  $C_M$ , and  $(C_L/C_D)/|C_M|$ , respectively.

**Table 5.** Parametric S/N ratio results of L16 orthogonal array.

Model Number	$C_L$	$C_D$	$C_M$	$C_L/C_D$	$(C_L/C_D)/ C_M $
1	0.9346	0.1028	−1.5635	9.0954	5.8173
2	0.9408	0.1022	−1.5510	9.2049	5.9348
3	0.9088	0.0999	−1.4685	9.0932	6.1923
4	0.9247	0.1028	−1.4710	8.9982	6.1170
5	0.9087	0.0999	−1.4550	9.0963	6.2517
6	0.9288	0.1007	−1.6353	9.2284	5.6433
7	0.9392	0.1027	−1.5260	9.1485	5.9951
8	0.9425	0.1032	−1.5683	9.1332	5.8237
9	0.9391	0.1019	−1.5642	9.2175	5.8928
10	0.9376	0.1022	−1.5544	9.1776	5.9042
11	0.9494	0.1030	−1.5991	9.2190	5.7652
12	0.9364	0.1012	−1.6543	9.2579	5.5964
13	0.9407	0.0995	−1.6221	9.4563	5.8296
14	0.9590	0.1020	−1.6726	9.4037	5.6221
15	0.9607	0.1016	−1.6861	9.4608	5.6109
16	0.9501	0.1045	−1.6706	9.0953	5.4442

Taguchi analysis predicted that for the  $C_L/C_D$  response, the sweep angle has the highest significance followed by twist angle, taper ratio, and tip angle, as shown in Table 6. The above prediction is examined for  $C_L/C_D$ , which is considered based on the larger-the-better criterion, and the variations in the S/N ratio for different parameters at the  $C_L/C_D$  condition is shown in Figure 11. As expected,  $C_M$  is influenced the most by tip angle, followed by sweep angle, twist angle, and taper ratio, as shown in Table 7. Overall, the cant angle is the most important parameter for the aerodynamic coefficients. This prediction is observed for the  $C_M$  response, which is considered based on the smaller-the-better criterion,

and the variations in the S/N ratio for different parameters at the  $C_M$  condition is shown in Figure 12. The variations in the S/N ratio for different parameters at the dependent parameter  $(C_L/C_D)/|C_M|$  condition is shown in Figure 13, which shows the predicted response  $(C_L/C_D)/|C_M|$ , which is highly influenced by tip angle, followed by tip ratio, sweep angle, and taper angle based on the larger-the-better criterion, as shown in Table 8.

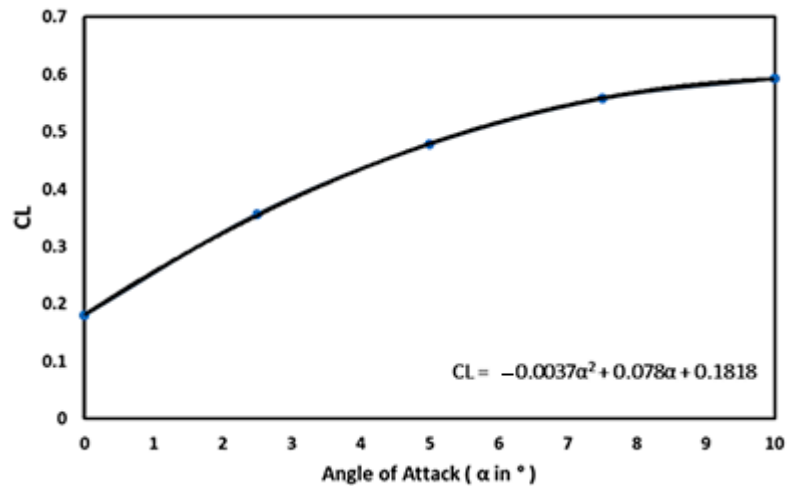


Figure 10. Effect of attack angle on lift coefficient for NASA CRM at  $Re = 5 \times 10^6$ .

Table 6. S/N ratio response and parameter rankings for  $C_L/C_D$ .

Symbol	Design Parameters	Level 1	Level 2	Level 3	Level 4	Max-Min	Rank
A	Cant angle of the first tip	19.10	19.15	19.11	19.05	0.10	4
B	Taper ratio	19.04	19.08	19.12	19.17	0.14	3
C	Sweep angle	19.09	19.27	19.18	18.86	0.42	1
D	Tip Twist	19.00	19.12	19.19	19.09	0.19	2
Average $C_L/C_D$ Value = 19.1013							

Table 7. S/N ratio response and parameter rankings for  $C_M$ .

Symbol	Design Parameters	Level 1	Level 2	Level 3	Level 4	Max-Min	Rank
A	Cant angle of the first tip	−3.596	−3.909	−4.042	−4.416	0.820	1
B	Taper ratio	−3.938	−4.096	−3.906	−4.023	0.190	4
C	Sweep angle	−4.172	−4.126	−3.900	−3.764	0.408	2
D	Tip Twist	−4.098	−4.000	−3.852	−4.012	0.246	3
Average $C_M$ value = −3.9906							

Table 8. S/N ratio response and parameter rankings for  $(C_L/C_D)/|C_M|$ .

Symbol	Design Parameters	Level 1	Level 2	Level 3	Level 4	Max-Min	Rank
A	Cant angle of the first tip	15.50	15.24	15.07	14.63	0.87	1
B	Taper ratio	15.10	14.98	15.22	15.15	0.24	4
C	Sweep angle	14.92	15.15	15.28	15.09	0.36	3
D	Tip Twist	14.91	15.12	15.34	15.08	0.44	2
Average $(C_L/C_D)/ C_M $ value = 15.1113							

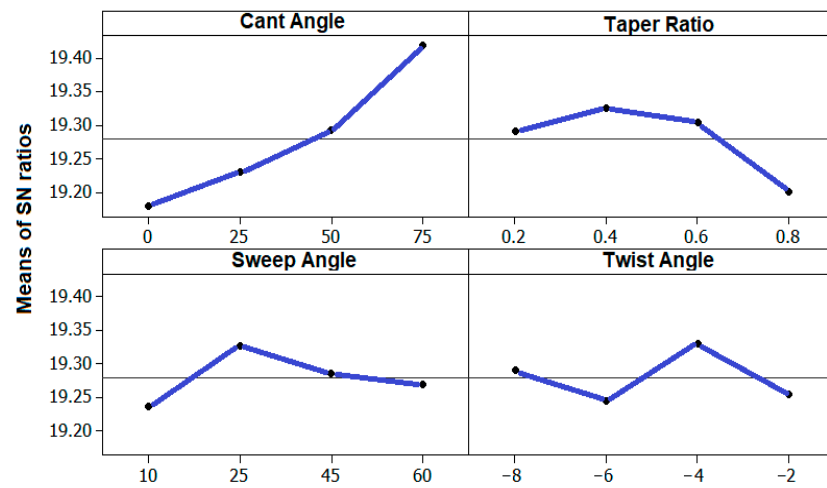


Figure 11. Variations in S/N ratios for different parameters at the  $C_L/C_D$  condition.

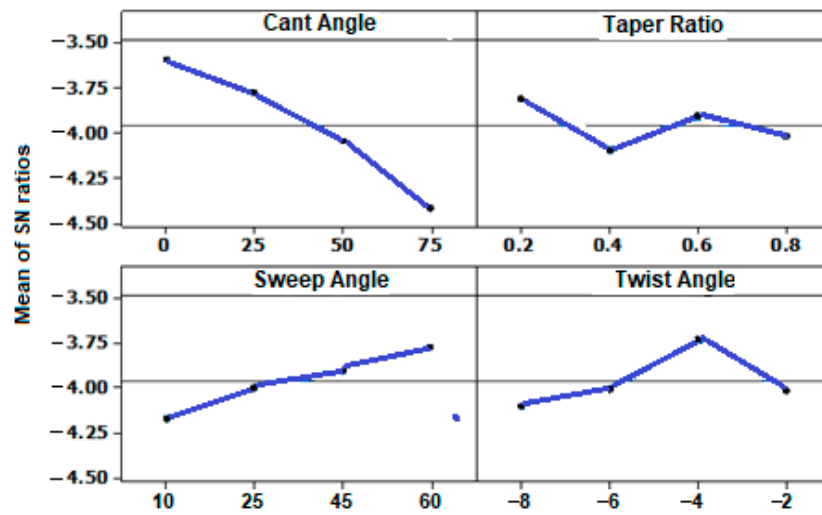


Figure 12. Variations in S/N ratios for different parameters at the  $C_M$  condition.

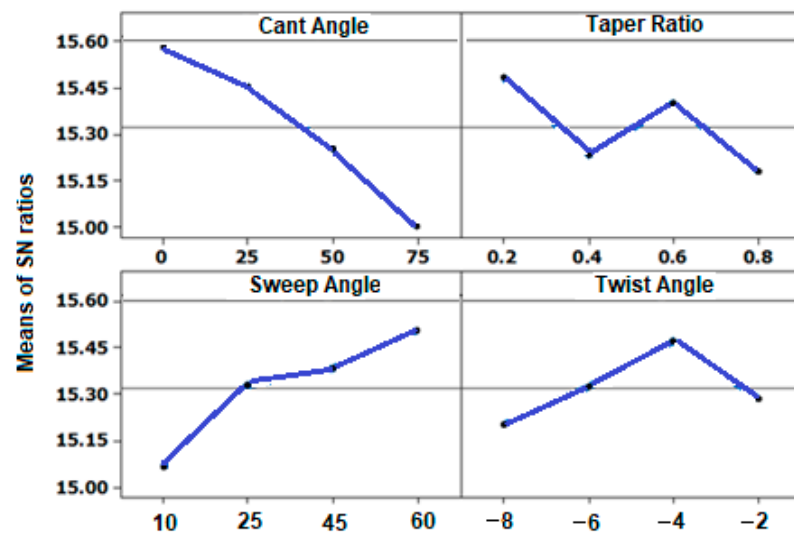


Figure 13. Variations in S/N ratios for different parameters at the  $(C_L/C_D)/|C_M|$  condition.

### 5.3. Analysis of Variance (ANOVA) of Winglet Design Using the Taguchi Method

ANOVA analysis is performed to determine the percentage contribution of each design parameter of the winglet design at a confidence level of 95%. Tables 9–11 shows the contribution of each parameter to the dependent parameters,  $C_L/C_D$ ,  $C_M$ , and  $(C_L/C_D)/|C_M|$ . It is observed from Figure 14 that the cant angle is the most contributing parameter with percentages of 53.97, 59.36, and 65.31 for the dependent parameters  $C_L/C_D$ ,  $C_M$ , and  $(C_L/C_D)/|C_M|$ , respectively. The taper ratio is the least influencing parameter for  $C_M$ , which has a contribution of 4.21%. In the case of  $C_L/C_D$ , the sweep angles have a contribution of 6.93%, which is the least, as well as lower than the error contribution. This denotes another possible significant design parameter whose contribution is more than the sweep angle for  $C_L/C_D$ . It is also observed that the Taguchi method and ANOVA determined the same order of significance. For  $C_L/C_D$ , the contribution of sweep angle is less than the error percentage, denoting some other parameter or combination of parameters that influences the aerodynamic efficiency more than the sweep angle. Additionally, the effect levels of winglet design parameters of a transonic wing on  $(C_L/C_D)$  and  $C_M$  are identified using the analysis of variance. For  $C_M$ , the contribution of error percentage is less than the other input parameters; i.e., all the input parameters are involved to decide the optimum response of  $C_M$  for the winglet design of the transonic wing, even though the cant angle is the most influential parameter on the transonic wing design, followed by sweep angle, twist angle, and, finally, the taper ratio, which define the optimum response of the  $C_M$  value.

**Table 9.** ANOVA analysis for  $C_L/C_D$  ratio.

Source	Degree of Freedom	Sum of Square (SS)	Contribution %
$\Phi$	3	0.146801	53.97
$\lambda$	3	0.040654	14.95
$\Delta$	3	0.018837	6.93
$\epsilon$	3	0.044946	16.52
Error	3	0.020749	7.63
Total	15	0.271988	100

**Table 10.** ANOVA analysis for  $C_M$ .

Source	Degree of Freedom	Sum of Square (SS)	Contribution %
$\Phi$	3	0.0409	59.36
$\lambda$	3	0.0052	7.61
$\Delta$	3	0.0095	13.75
$\epsilon$	3	0.0087	12.56
Error	3	0.0046	6.72
Total	15	0.0689	100

**Table 11.** ANOVA for  $(C_L/C_D)/|C_M|$ .

Source	Degree of Freedom	The Sum of Square (SS)	Contribution %
$\Phi$	3	0.4752	44.90
$\lambda$	3	0.1497	14.14
$\Delta$	3	0.2546	24.06
$\epsilon$	3	0.1045	9.87
Error	3	0.0744	7.03
Total	15	1.0584	100

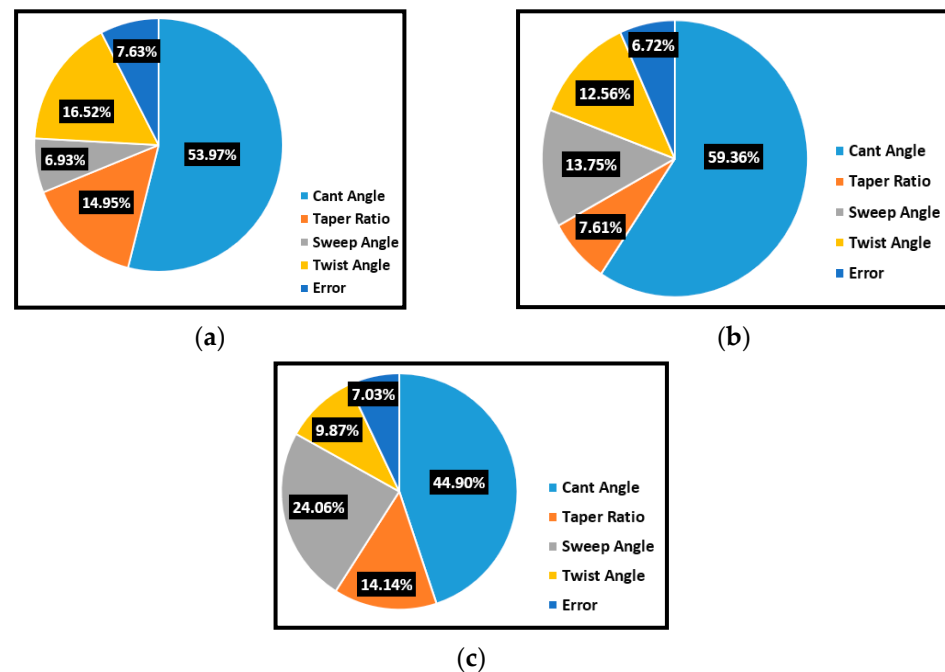


**Figure 14.** Contribution of design parameters on (a)  $C_L/C_D$ , (b)  $C_M$ , and (c)  $(C_L/C_D)/|C_M|$ .

Similarly, for the response  $(C_L/C_D)/|C_M|$ , the contribution of error percentage is less than the other input parameters considered for this transonic wing design, which results in the optimum response of  $(C_L/C_D)/|C_M|$ . From Table 11 and Figure 14, the cant angle is the most dominant parameter in the transonic wing design followed by sweep angle, taper ratio, and twist angle, which determine the optimum dependent response parameter of the  $C_M$  value.

#### 5.4. Taguchi—Grey Relational Analysis Coupled with Principal Component Analysis

The multi-input, discrete, and uncertain data problems are compactly analyzed by grey relational analysis (GRA), which gives the relationship between known and unknown information. This analysis appraises the absolute difference between data sequences while predicting the approximate grade of correlation between the responses. The grey relational grade (GRG) computes the degree of influence of similar sequences with the reference sequences [42]. GRA substantially aims to convert the multiple responses into single GRG values of all the trails. GRA synergizes with principal component analysis (PCA) in optimizing the process parameters in order to optimize the responses by finding the weightage of the responses, which determines the good results anticipated [43–45]. The designing and analysis of the transonic wing can be performed under several design parameters and with various responses of the winglet. In this study, to achieve the optimum responses of the transonic design, the Taguchi-based grey relational analysis (GRA) coupled with principal component analysis (PCA) for multi-response optimization are applied to improve the performance of the winglet design in the transonic wing. The grey relational grade (GRG) is used to identify the relationship between parameters in the sequence [46].

A higher GRG value level informs the optimum parameter levels in winglet design for maximizing the  $C_L/C_D$  ratio (the larger-the-better concept) and minimizing the  $C_M$  (the smaller-the-better) value. The reduction in variability in the experimental data are initially normalized, which is known as data preprocessing, and it helps to reduce the large variations in the responses between other responses. In other words, the normalizing experimental responses lie in the range of 0 to 1 [47]. Due to the above reason, two different approaches are discussed, depending on the characteristics of the data sequence, which may be either the larger-the-better or the smaller-the-better concept.



For the larger-the-better concept, the sequence is normalized using the following equation:

$$x_i(k)^* = \frac{x_i(k) - x_i(k)^-}{x_i(k)^+ - x_i(k)^-} \tag{3}$$

For the smaller-the-better concept, the sequence is normalized using the following equation:

$$x_i(k)^* = \frac{x_i(k)^+ - x_i(k)}{x_i(k)^+ - x_i(k)^-} \tag{4}$$

$x_i(k)^*$  is the normalised response,  $x_0(k)$  is the desired response,  $x_i(k)^+$  is the maximum of  $x_i(k)$ , and  $x_i(k)^-$  is the minimum of  $x_i(k)$ .

After pre-processing of the data, the corresponding grey relational coefficient (GRC) is calculated to express the relationship between the predicted and the actual experimental responses of the experiments. The grey relational coefficient  $\zeta_i(k)$  can be calculated using the following equation:

$$\zeta_i(k) = \frac{\Delta_{min} + \psi\Delta_{max}}{\Delta_{oi}(k) + \psi\Delta_{max}} \tag{5}$$

where the difference in the absolute value  $x_0(k)$  and  $x_i(k)$  is  $\Delta_{oi} = \|x_0(k) - x_i(k)\|$ .

The smallest value of  $\Delta_{oi}$ ,  $\Delta_{min} = \min_{\forall j \in i} \min_{\forall k} \|x_0(k) - x_j(k)\|$ .

The largest value of  $\Delta_{oi}$ ,  $\Delta_{max} = \max_{\forall j \in i} \max_{\forall k} \|x_0(k) - x_j(k)\|$ , and the distinguishing coefficient,  $\zeta = 0.5$ , is widely accepted for the analysis [41].

The experimental results are primarily used to obtain S/N ratios for the performance characteristics to examine the required effect with the best performance and the smallest variance. In this work,  $C_L/C_D$  is considered with the larger-the-better concept, while  $C_M$  is for the smaller-the-better concept for the winglet design of the transonic wing. All the original sequences of the S/N ratio in Table 12 are then substituted in Equations (3) and (4) to obtain normalised values of  $C_L/C_D$  and  $C_M$ , respectively. According to Palani et al. [41], larger values of the normalised results correspond to better performance, and the maximum normalised results equal to 1 indicate the best performance. The estimated values of normalized responses with their corresponding grey relational coefficients are based on Equation (6), which are shown in Table 12.

**Table 12.** Normalized responses and grey relational coefficients of responses.

Model Number	Normalized Responses		Grey Relational Coefficient (GRC)	
	$C_L/C_D$	$C_M$	$C_L/C_D$	$C_M$
1	0.2101	0.4695	0.3876	0.4852
2	0.4468	0.4154	0.4748	0.4610
3	0.2054	0.0584	0.3862	0.3468
4	0.0000	0.0692	0.3333	0.3495
5	0.2121	0.0000	0.3882	0.3333
6	0.4976	0.7802	0.4988	0.6946
7	0.3249	0.3072	0.4255	0.4192
8	0.2918	0.4903	0.4138	0.4952
9	0.4741	0.4725	0.4874	0.4866
10	0.3878	0.4301	0.4496	0.4673
11	0.4773	0.6235	0.4889	0.5705
12	0.5614	0.8624	0.5327	0.7842
13	0.9903	0.7231	0.9809	0.6436
14	0.8766	0.9416	0.8020	0.8954
15	1.0000	1.0000	1.0000	1.0000
16	0.2099	0.9329	0.3876	0.8817

Principal component analysis (PCA) is applied to examine the weightage of each response of the winglet design to imitate its relative importance in the grey relational analysis. Equation (6) is used to produce the correlation coefficient matrix for eigenvalue and eigenvector determination based on Table 9 and the grey relational coefficients of the responses of  $C_L/C_D$  and  $C_M$ .

$$N_{k,l} = \frac{Cov(x_i(k), x_i(l))}{\sqrt{Var(x_i(k)) \cdot Var(x_i(l))}} \tag{6}$$

where  $k = 1, 2, \dots, n$ , and  $l = 1, 2, \dots, n$ .

$Cov(x_i(k), x_i(l))$  is the covariance of sequence  $x_i(k)$  and  $x_i(l)$ ,  $Var(x_i(k))$  is the standard deviation of sequence  $x_i(k)$ , and  $Var(x_i(l))$  is the standard deviation of sequence  $x_i(l)$ .

The eigenvalues and eigenvectors are determined from the Covariance matrix array using the following equation:

$$(N_{k,l} - \lambda_k I_m) V_{i,k} = 0 \tag{7}$$

where  $N$  is the correlation coefficient matrix form of  $N_{kl}$ ,  $\lambda_k$  is the  $k$ th eigenvalue,  $\sum_{k=1}^n \lambda_k = n$ ,  $k = 1, 2, \dots, n$ , and  $V_{i,k} = [a_{k1}, a_{k2}, \dots, a_{kn}]^T$  is the eigenvector corresponding to the eigenvalue  $\lambda_k$ .

Using Equation (7), the eigenvalues are determined from the correlation coefficient matrix of the grey relational coefficients of the transonic wing design and are shown in Table 13. The eigenvectors and contribution of winglet design responses corresponding to each eigenvalue are enumerated in Table 14.

**Table 13.** Eigenvalues and explained variations for principal components of responses.

Principal Component	Eigenvalues	Explained Variation (%)
First	1.7055	85.28
Second	0.2945	14.72

**Table 14.** Eigenvectors for principal components of winglet design responses.

Responses	Eigenvectors		
	First Principal Component	Second Principal Component	Contribution
$C_L/C_D$	-0.7071	-0.7071	0.4999
$C_M$	0.7071	-0.7071	0.4999

The weighting values of the responses are determined by principal component analysis, and the following equation gives the weighted grey relational grade of all the responses:

$$\gamma_i = \frac{1}{n} \sum_{k=1}^n (\omega_k \cdot \zeta_i(k)) \tag{8}$$

where  $i = 1, 2, \dots, m$ , and  $k = 1, 2, \dots, n$ .

$\omega_k$  is the weighting factor for the response  $k$ , which is estimated through principal component analysis. The relational degree between the ideal sequence  $x_0(k)$  and the given sequence  $x_i(k)$  is stronger the higher the grey relational grade.

The first principal component has high variance contribution characteristics of 85.28% compared to other principal components. Furthermore, the squares of its corresponding eigenvectors are designated as the weighting values of  $C_L/C_D$  and  $C_M$ , which are 0.4999 and 0.4999, respectively. Using Equation (8), the weighted grey relational grades and their corresponding ranks are calculated as shown in Table 15.

**Table 15.** Grey relational grades and their respective ranking orders.

Model Number	Weighted Grey Relational Grade (WGRG)	Rank
1	0.3151	13
2	0.3526	9
3	0.2798	14
4	0.2540	16
5	0.2774	15
6	0.4230	5
7	0.3175	12
8	0.3307	11
9	0.3653	8
10	0.3415	10
11	0.3870	7
12	0.4623	4
13	0.6512	2
14	0.6247	3
15	0.7499	1
16	0.4141	6

Thus, the optimization process is performed with respect to a single weighted grey relational grade rather than complex responses of the winglet design. Figure 15 shows the weighted grey relational grade (WGRG) graph, which shows the variations in WGRG in each experimental trial, and model number 15 has the highest weighted grey relational grade of 0.7499. On the winglet design responses, higher weighted grey relational grades generally result into better multiple performances.

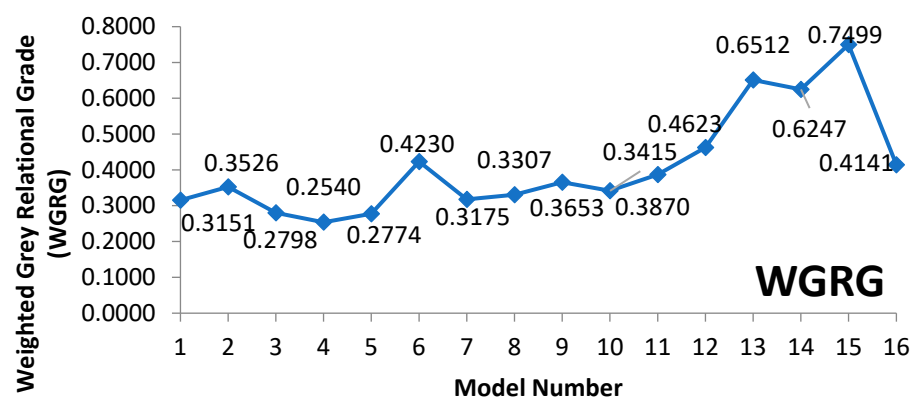


**Figure 15.** Graphical representation of WGRG.

The regression model of the weighted grey relational grade is defined by using the following equation:

$$WGRG = 0.214461 + 0.0981\phi - 0.0113\lambda - 0.0042\Lambda - 0.0045C \tag{9}$$

Hence, the higher level of mean responses of the transonic wing is selected as the optimum condition of the winglet design. The best combination of the winglet design of transonic design is identified with A4 (cant angle of 75°), B2 (taper ratio of 0.2), C2 (sweep angle of 25°), and D2 (tip twist of −2°) from the 16 combinations of the experiments. Thus, the optimum value of WGRG is estimated based on the literature [44]. The response table for the weighted grey relational grades shown in Table 16 and Figure 16 shows the predicted response weighted grey relational grade that is highly influenced by the cant angle, followed by the twist angle, sweep angle, and taper angle based on the larger-the-better criterion.

Table 16. Response table for weighted grey relational grade (WGRG).

Symbol	Design Parameters	Level 1	Level 2	Level 3	Level 4	Max-Min	Rank
A	Cant angle of the first tip	0.3003	0.3371	0.3890	0.6100	0.3096	1
B	Taper ratio	0.4022	0.4355	0.4335	0.3653	0.0702	4
C	Sweep angle	0.3848	0.4605	0.4001	0.3911	0.0757	3
D	Tip Twist	0.4299	0.4304	0.3282	0.4480	0.1198	2

Average Weighted Grey Relational Grade = 0.4091

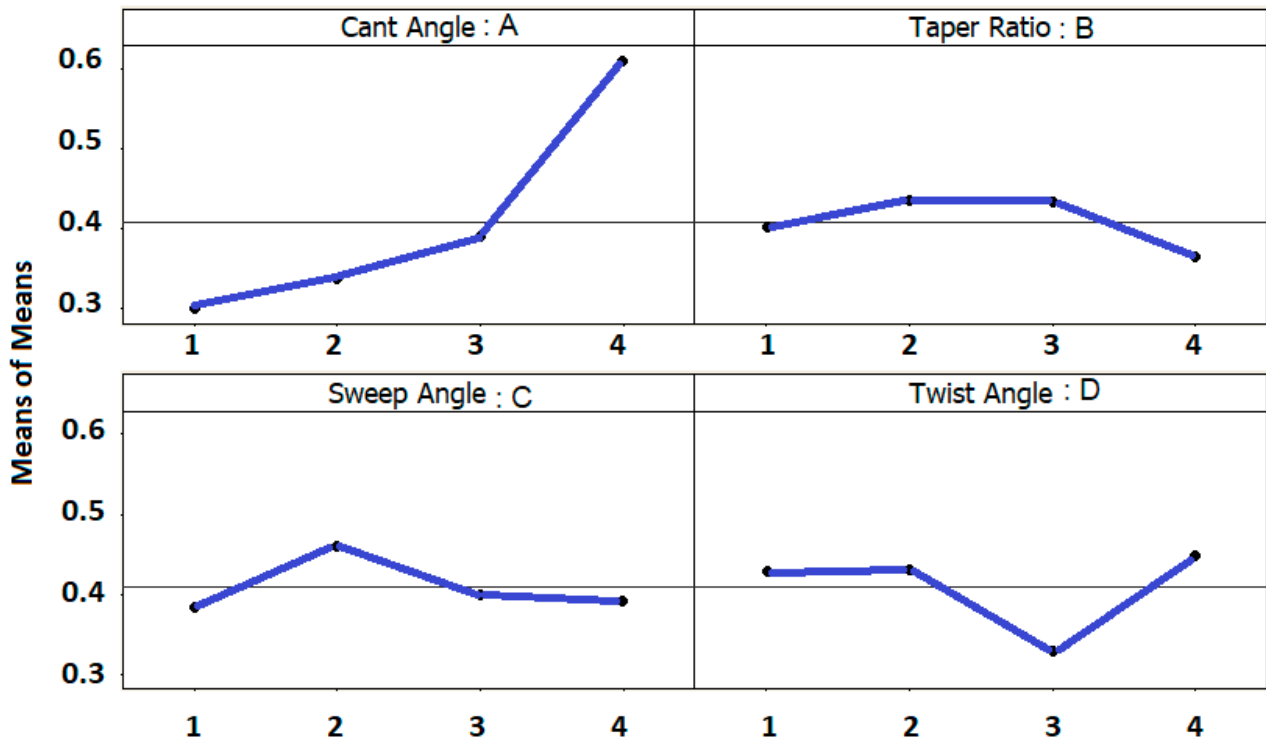


Figure 16. Means for weighted grey relational grade.

5.5. ANOVA of Winglet Design Using TGRA Coupled with PCA

Significant input process parameters are investigated using the ANOVA in the winglet design of the transonic wing. The sum of the squared deviations of the present work is measured by separating the variability of the weighted grey relational grade with a reduction in error. This method shows the major contributing responses in the transonic wing design and how the input process parameters affect the responses to achieve optimum results.

The results of ANOVA for the weighted grey relational grade are listed in Table 17. It shows that the sweep angle is the most dominant process parameter affecting the multiple responses due to its highest percentage contribution among the process parameters, followed by twist angle, cant angle, and taper ratio, respectively. It may be noted that the minimum error percentage on the responses is observed. The appearance of the minimum error percentage indicates that the effects of all the input process parameters involved in different weightage are mostly involved to obtain the optimum output responses of the design [48,49].

**Table 17.** Analysis of variance for grey relational grade.

Source	SS	DOF	Adj SS	Adj MS	F Ratio	p Value	Remarks	Contribution (%)	
Cant angle of the first tip, A	0.05299	3	0.05299	0.01766	138.66	0.001	Significant	22.864	
Taper ratio, B	0.02387	3	0.02387	0.00796	62.47	0.003	Significant	10.299	
Sweep angle, C	0.09853	3	0.09853	0.03284	257.85	0.001	Significant	42.514	
Tip Twist, D	0.05599	3	0.05599	0.01866	146.51	0.001	Significant	24.159	
Error	0.00038	3	0.00038	0.00013				0.164	
Total	0.23176	15							
S = 0.0112860		R-Sq = 99.84%				R-Sq(adj) = 99.18%			

The improvement in the responses of the transonic design at the optimal conditions is verified after obtaining the optimal level of the winglet design parameters of the transonic design. Table 18 compares the results of the confirmation experiments using the optimal winglet design parameters (A4, B2, C2, D2) obtained by the proposed methods and those of the initial design parameters (A1, B1, C1, D1). From Table 15,  $C_L/C_D$  increases from 0.9214 to 0.9509,  $C_M$  decreases from 0.1042 to 0.1022, and  $(C_L/C_D)/|C_M|$  increases from 5.6556 to 6.3320. Accordingly, these confirmation tests reveal that the proposed optimum method for solving the optimal combinations of the design parameters in this work improves the  $C_L/C_D$ ,  $C_M$ , and  $(C_L/C_D)/|C_M|$  of the transonic wing. The optimized dependent design parameter,  $(C_L/C_D)/|C_M|$ , is examined with an improvement of 20.771% compared to other models such as NASA CRM and blended models for the design parameters viz. the first tip cant angle of  $75^\circ$ , taper ratio of 0.4, sweep angle of  $25^\circ$ , and tip twist angle of  $-6^\circ$ , as shown in Table 19. Figure 17 shows the front view and top views of the winglet design at the optimum input conditions.

**Table 18.** Comparison between initial level and optimum level.

	Best Combination	$C_L$	$C_D$	$C_M$	$C_L/C_D$	$(C_L/C_D)/ C_M $
Initial design	A1B1C1D1	0.9214	0.1042	-1.5635	8.8426	5.6556
Optimal design	A4B2C2D2	0.9509	0.1022	-1.4896	9.2540	6.3320
Improvement (%)	-	3.202	1.957	4.961	4.652	11.960

**Table 19.** Comparison of optimized design, blended, and NASA CRM.

Model	$C_L$	$C_D$	$C_M$	$C_L/C_D$	$(C_L/C_D)/ C_M $	$(C_L/C_D)/ C_M $ Improvement (%)
NASA CRM	1	0.1133	-1.685	8.821	5.243	-
Blended	0.913	0.1016	-1.5268	8.992	5.891	12.359
Optimized Design	Taguchi	0.916	0.1024	-1.4439	8.948	18.291
	T-GRA with PCA	0.9509	0.1022	-1.4896	9.254	20.771

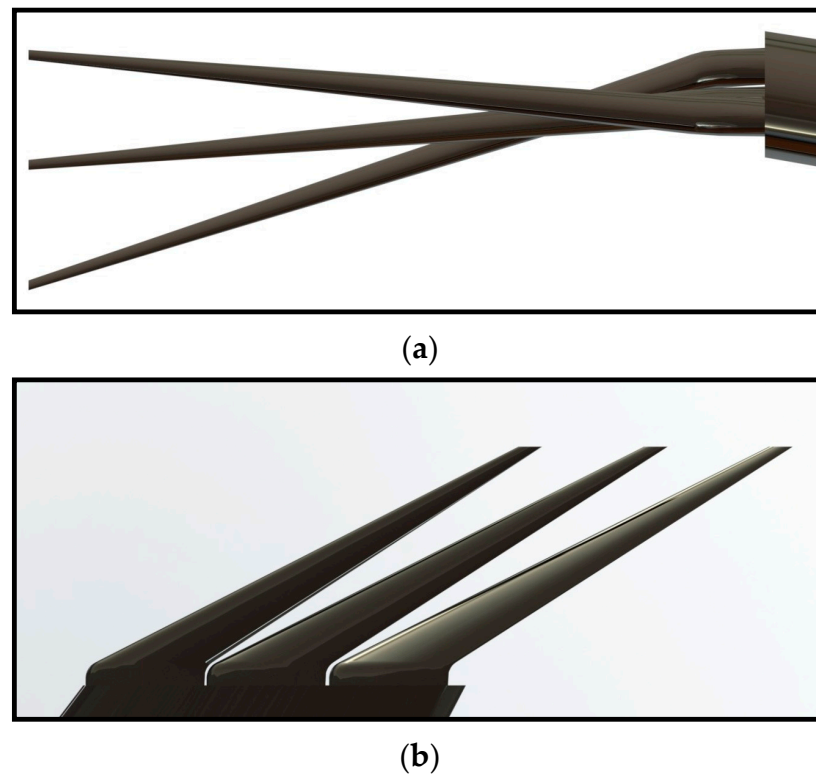


Figure 17. (a) Front view and (b) top view of the optimized winglet.

## 6. Conclusions

This present numerical study was focused on reducing induced drag acting on a commercial transport NASA CRM wing model. A typical industrial retrofitting approach was carried out throughout our design process; i.e., winglets were attached at the end of the wing while maintaining the span constant. Unconventional winglet designs such as twisted, multi-tip, and bird-type winglets were analyzed to understand their flow behaviour and determine their aerodynamic performance. Furthermore, a parametric study was carried out on a multi-tip winglet design. Four important design parameters, cant angle, sweep angle, tip twist angle, and taper ratio, were investigated to understand their relative importance and optimize their design using the Taguchi method and Taguchi-based grey relational analysis coupled with principal component analysis. Moreover, the percentage of the contribution of each parameter to dependent parameters was determined through ANOVA analysis.

This study found the  $C_M$  for the wing's root at the quarter chord location. In this study, an optimal winglet design was developed by maximizing  $(C_L/C_D)/|C_M|$ , and an optimal aerodynamic design was developed while considering the wing root bending moment. Some of this study's important findings are listed below.

- A multi-tip winglet performs better than other winglet designs.
- $\Phi$  is the most important parameter and contributes around 45–60% to aerodynamic coefficients  $C_L$ ,  $C_D$ , and  $C_M$ .
- The proposed optimum method for the selected design parameters in this work improves the  $C_L/C_D$ ,  $C_M$ , and  $(C_L/C_D)/|C_M|$  of a transonic wing.
- In the Taguchi technique, the optimised multi-tip winglet based on  $(C_L/C_D)/|C_M|$  improved by 18.291%, and in T-GRA combined with the PCA approach, it improved by 20.771%. Furthermore, it exceeded the blended winglet by 8% and the baseline wing by 6%, respectively.
- The optimized design has cant angle first-tip =  $75^\circ$ , taper ratio = 0.4, sweep angle =  $25^\circ$  and tip twist =  $-6^\circ$ .

- The relative importance of parameters for high  $C_L/C_D$  is cant angle ( $\Phi$ ) > sweep angle ( $\Lambda$ ) > tip twist ( $\epsilon$ ) > taper ratio ( $\lambda$ ), and for high  $C_L/C_D/|C_M|$ , it is  $\Phi > \Lambda > \lambda > \epsilon$ .

**Author Contributions:** Conceptualization, P.P. and A.S.; methodology, numerical analysis, and validation, S.A., P.P. and A.S., P.R.K. and N.R.D.; writing—original draft, P.P., A.S., S.A., K.P., P.R.K. and N.R.D.; supervision P.R.K., P.P. and J.T.; writing—review and editing, P.P., A.S., S.A., K.P., P.R.K., N.R.D., D.T. and T.S.; formal analysis, T.S., A.S., P.P. and P.R.K.; data curation, B.W. All authors have read and agreed to the published version of the manuscript.

**Funding:** This research received no external funding.

**Institutional Review Board Statement:** Not applicable.

**Informed Consent Statement:** Not applicable.

**Data Availability Statement:** The raw data supporting the conclusions of this article will be made available by the authors on request.

**Conflicts of Interest:** The authors declare no conflicts of interest.

## References

- Gavrilović, N.N.; Rašuo, B.P.; Dulikravich, G.S.; Parezanović, V.B. Commercial aircraft performance improvement using winglets. *FME Trans.* **2014**, *43*, 1–8. [CrossRef]
- Whitcomb, R.T. *A Design Approach and Selected Wind-Tunnel Results at High Subsonic Speeds for Wing-Tip Mounted Winglets*; NASA N D-8260; NASA: Washington, DC, USA, 1976.
- Azmi, A.M.; Taib, C.F.M.; Kasolang, S.; Muhammad, F.H. CFD Analysis of Winglets at Low Subsonic Flow. In Proceedings of the World Congress on Engineering, London, UK, 6–8 July 2011.
- Elham, A.; van Tooren, M.J. Winglet multi-objective shape optimization. *Aerosp. Sci. Technol.* **2014**, *37*, 93–109. [CrossRef]
- Hossain, A.; Rahman, A.; Hossen, J.; Iqbal, A.K.M.P.; Zahirul, M.I. Prediction of aerodynamic characteristics of an aircraft model with and without winglet using fuzzy logic technique. *Aerosp. Sci. Technol.* **2011**, *15*, 595–605. [CrossRef]
- Khalil, E.E.; Helal, H.; Abdellatif, O.; ElHarriri, G.M. Aircraft Blended Winglet Performance Analyses. In Proceedings of the 55th AIAA Aerospace Sciences Meeting, Grapevine, TX, USA, 9–13 January 2017; p. 1838. [CrossRef]
- Lee, T.; Gerontakos, P. Effect of Winglet Dihedral on a Tip Vortex. *J. Aircr.* **2012**, *43*, 117–124. [CrossRef]
- Aubeelack, H.; Botez, R.M. Simulation Study of the Aerodynamic Force Distributions on the UAS-S45 Baalam Wing with an Upswept Blended Winglet. *Incas Bull.* **2019**, *11*, 21–38. [CrossRef]
- Reddy, T.R.; Patil, P.M.; Reddy, G.S. Modeling and CFD Analysis of Flow over Aircraft Split Winglet and Blended Winglet. *Int. J. Adv. Sci. Res. Eng.* **2018**, *4*, 88–93. [CrossRef]
- Madhanraj, V.; Chandra, K.G.; Swprazeeth, D.; Gopal, B.D. Design and Computational Analysis of Winglets. *Turk. J. Comput. Math. Educ.* **2021**, *12*, 1–9. Available online: <https://turcomat.org/index.php/turkbilmat/article/view/2530> (accessed on 3 May 2022).
- Seshaiah, T.; Vasu, B.; Reddy, K.V.K.; Bridjesh, P. Analysis on aircraft winglets at different angles by using CFD simulation. *Mater. Today Proc.* **2021**, *49*, 275–283. [CrossRef]
- Reddy, S.R.; Dulikravich, G.S.; Abdoli, A.; Sobieczky, H. Multi-Winglets: Multi-Objective Optimization of Aerodynamic Shapes. In Proceedings of the 53rd AIAA Aerospace Sciences Meeting, Kissimmee, FL, USA, 5–9 January 2015; p. 1489. [CrossRef]
- Ilie, M.; White, M.; Soloiu, V.; Rahman, M. The effect of winglets on the aircraft wing aerodynamics; numerical studies using LES. In Proceedings of the AIAA Scitech 2019 Forum, San Diego, CA, USA, 7–11 January 2019; p. 1308. [CrossRef]
- Ning, A.; Kroo, I. Tip Extensions, Winglets, and C-wings: Conceptual Design and Optimization. In Proceedings of the 26th AIAA Applied Aerodynamics Conference, Honolulu, HI, USA, 18–21 August 2008. [CrossRef]
- Pfeiffer, N.J. Numerical Winglet Optimization. In Proceedings of the 42nd AIAA Aerospace Sciences Meeting, Reno, NV, USA, 5–8 January 2004; p. 213. [CrossRef]
- Eguea, J.P.; da-Silva, G.P.G.; Catalano, F.M. Fuel efficiency improvement on a business jet using a camber morphing winglet concept. *Aerosp. Sci. Technol.* **2019**, *96*, 105542. [CrossRef]
- Ishimitsu, K. Aerodynamic Design and Analysis of Winglets. In Proceedings of the AIAA Aircraft Systems and Technology Meeting, Dallas, TX, USA, 27–29 September 1976. [CrossRef]
- Panagiotou, P.; Kaparos, P.; Yakinthos, K. Winglet design and optimization for a MALE UAV using CFD. *Aerosp. Sci. Technol.* **2014**, *39*, 190–205. [CrossRef]
- El Haddad, N.R.; Gonzalez-Linero, L. Aerodynamic Design of a Winglet for the Dassault Falcon 10 USA. In Proceedings of the 54th AIAA Aerospace Sciences Meeting, San Diego, CA, USA, 4–8 January 2016. [CrossRef]
- Catalano, F.M.; Ceron-Muñoz, H.D. Experimental Analysis Of Aerodynamics Characteristics Of Adaptive Multiwinglets. In Proceedings of the 43rd AIAA Aerospace Sciences Meeting and Exhibit, Reno, NV, USA, 10–13 January 2005; p. 1231.

21. Smith, M.; Komerath, N.; Ames, R.; Wong, O.; Pearson, J. Performance Analysis of a Wing With Multiple Winglets. In Proceedings of the 19th AIAA Applied Aerodynamics Conference, Anaheim, CA, USA, 11–14 June 2001. [[CrossRef](#)]
22. Shelton, A.; Tomar, A.; Prasad, J.V.R.; Smith, M.J.; Komerath, N. Active Multiple Winglets for Improved Unmanned-Aerial-Vehicle Performance. *J. Aircr.* **2006**, *43*, 110–116. [[CrossRef](#)]
23. Takenaka, K.; Hatanaka, K.; Yamazaki, W.; Nakahashi, K. Multidisciplinary Design Exploration for a Winglet. *J. Aircr.* **2008**, *45*, 1601–1611. [[CrossRef](#)]
24. Zhang, L.; Dongli, M.A.; Yang, M.; Wang, S. Optimization and analysis of winglet configuration for solar aircraft. *Chin. J. Aeronaut.* **2020**, *33*, 3238–3252. [[CrossRef](#)]
25. Samuel, M.S.G.; Rajendran, P. A Review of Winglets on Tip Vortex, Drag and Airfoil Geometry. *J. Adv. Res. Fluid Mech. Therm. Sci.* **2019**, *63*, 218–237.
26. McLean, D. Wingtip Devices: What They Do and How They Do It. In Proceedings of the Boeing Performance and Flight Operations Engineering Conference, Seattle, WA, USA, 2005; Available online: [https://www.smartcockpit.com/docs/Wingtip\\_Devices.pdf](https://www.smartcockpit.com/docs/Wingtip_Devices.pdf) (accessed on 3 May 2022).
27. Palani, K.; Elanchezian, C.; Bhaskar, G.B. Multi Response DEA-Based Taguchi Optimization of Process Parameters on AA8011 Friction Stir Welded Aluminium Alloys. *Appl. Mech. Mater.* **2015**, *766–767*, 921–927. [[CrossRef](#)]
28. Vassberg, J.; Dehaan, M.; Rivers, M.; Wahls, R. Development of a Common Research Model for Applied CFD Validation Studies. In Proceedings of the 26th AIAA Applied Aerodynamics Conference, Honolulu, HI, USA, 18–21 August 2008. [[CrossRef](#)]
29. Narayan, G.; John, B. Effect of winglets induced tip vortex structure on the performance of subsonic wings. *Aerosp. Sci. Technol.* **2016**, *58*, 328–340. [[CrossRef](#)]
30. Rajendran, S. Design of Parametric Winglets and Wing Tip Devices—A Conceptual Design Approach. 2012. Available online: <https://www.divaportal.org/smash/get/diva2:547954/Fulltext01.pdf> (accessed on 3 May 2022).
31. Abdelghany, E.S.; Khalil, E.E.; Abdellatif, O.E.; Elhariry, G. Air Craft Winglet Design and Performance: Cant Angle Effect. *J. Robot. Mech. Eng. Resr.* **2016**, *1*, 28–34.
32. Spalart, P.; Allmaras, S. A one-equation turbulence model for aerodynamic flows. In Proceedings of the 30th Aerospace Sciences Meeting and Exhibit, Reno, NV, USA, 6–9 January 1992. [[CrossRef](#)]
33. Schmitt, V.; Charpin, F. *Pressure Distribution on the ONERA M6 Wing at Transonic Mach Numbers*; AGARD-AR-138; AGARD: Neuilly sur Seine, France, 1979.
34. Crovato, A.; Almeida, H.; Vio, G.A.; Silva, G.H.; Prado, A.P.; Breviglieri, C.; Guner, H.; Cabral, P.H.; Boman, R.; Terrapon, V.E.; et al. Effect of Levels of Fidelity on Steady Aerodynamic and Static Aeroelastic Computations. *Aerospace* **2020**, *7*, 42. [[CrossRef](#)]
35. Durrani, N.; Qin, N. Comparison of RANS, DES and DDES Results for ONERA M-6 Wing at Transonic Flow Speed Using an In-House Parallel Code. In Proceedings of the 49th AIAA Aerospace Sciences Meeting including the New Horizons Forum and Aerospace Exposition, Orlando, FL, USA, 4–7 January 2011; p. 190. [[CrossRef](#)]
36. Moigne, A.L. A Discrete Navier-Stokes Adjoint Method for Aerodynamic Optimization of Blended Wing-Body Configurations. Ph.D. Thesis, Cranfield University, Bedford, UK, 2002.
37. Neilsen, E.J.; Anderson, W.K. Recent Improvements in Aerodynamic Design Optimization on Unstructured Meshes. *AIAA Pap.* **2002**, *40*, 6. [[CrossRef](#)]
38. Rho, O.; Lee, K.; Kim, C.; Kim, C.; Lee, B. Parallelized Design Optimization for Transonic Wings using Aerodynamic Sensitivity Analysis. In Proceedings of the 40th AIAA Aerospace Sciences Meeting & Exhibit, Reno, NV, USA, 14–17 January 2002; p. 264. [[CrossRef](#)]
39. Radespiel, R.; Rossow, C.; Swanson, R.C. Efficient Cell-Vertex Multigrid Schemes for the Three-Dimensional Navier-Stokes Equations. *AIAA J.* **1990**, *28*, 1464–1472. [[CrossRef](#)]
40. Hyoungjin, K.; Oh-Hyun, R. Aerodynamic Design of Transonic Wings Using the Target Pressure Optimization Approach. *J. Aircr.* **1998**, *35*, 671–677. [[CrossRef](#)]
41. Palani, K.; Arunprasad, S. Multi response Optimization of Welding Parameters in Dissimilar Plasma Arc Welded Joints Using RSM Based GRA Coupled with PCA. *IOP Conf. Ser. Mater. Sci. Eng.* **2020**, *954*, 012034. [[CrossRef](#)]
42. Lu, H.S.; Chang, C.K.; Hwang, N.C.; Chung, C.T. Grey relational analysis coupled with principal component analysis for optimization design of the cutting parameters in high-speed end milling. *J. Mater. Process. Technol.* **2009**, *209*, 3808–3817. [[CrossRef](#)]
43. Tarnq, Y.S.; Juang, S.C.; Chang, C.H. The use of grey-based Taguchi methods to determine submerged arc welding process parameters in hardfacing. *J. Mater. Process. Technol.* **2002**, *128*, 1–6. [[CrossRef](#)]
44. Palani, K.; Elanchezian, C. Multi responses Optimization of Friction stir welding process parameters in dissimilar alloys using Grey relational analysis. *IOP Conf. Ser. Mater. Sci. Eng.* **2018**, *390*, 012061. [[CrossRef](#)]
45. Palani, K.; Elanchezian, C. Multi Response Optimization of Process Parameters on AA8011 Friction Stir Welded Aluminium Alloys using RSM Based GRA Coupled With DEA. *Appl. Mech. Mater.* **2015**, *813*, 446–450. [[CrossRef](#)]
46. Kavimani, V.; Prakash, K.S.; Thankachan, T.; Nagaraja, S.; Jeevanantham, A.K.; Jhon, J.P. WEDM Parameter Optimization for Silicon@r-GO/Magneisum Composite Using Taguchi Based GRA Coupled PCA. *Silicon* **2020**, *12*, 1161–1175. [[CrossRef](#)]
47. Ilkhechi, N.N.; Yavari, R.; Barakan, S. Evaluation and Optimization of Effective Parameters on Zinc Sulfate Flotation by the Taguchi Method. *Silicon* **2016**, *9*, 695–701. [[CrossRef](#)]



48. Pradhan, M.K. Estimating the effect of process parameters on MRR, TWR and radial overcut of EDMed AISI D2 tool steel by RSM and GRA coupled with PCA. *Int. J. Adv. Manuf. Technol.* **2013**, *68*, 591–605. [[CrossRef](#)]
49. Daniel, S.A.A.; Pugazhenth, R.; Kumar, R.; Vijayananth, S. Multi objective prediction and optimization of control parameters in the milling of aluminum hybrid metal matrix composites using ANN and Taguchi-grey relational analysis. *Def. Technol.* **2019**, *15*, 545–556. [[CrossRef](#)]

**Disclaimer/Publisher's Note:** The statements, opinions and data contained in all publications are solely those of the individual author(s) and contributor(s) and not of MDPI and/or the editor(s). MDPI and/or the editor(s) disclaim responsibility for any injury to people or property resulting from any ideas, methods, instructions or products referred to in the content.